Remote detection and recording of atomic-scale spin dynamics

Elbertse, R. J.G.; Coffey, D.; Gobeil, J.; Otte, A. F.

DOI
10.1038/s42005-020-0361-z

Publication date
2020

Document Version
Final published version

Published in
Communications Physics

COMMUNICATIONS PHYSICS

ARTICLE

https://doi.org/10.1038/s42005-020-0361-z OPEN

Remote detection and recording of atomic-scale spin dynamics

R. J. G. Elbertse [1,2], D. Coffey[1,2], J. Gobeil [1] & A. F. Otte [1✉]

Atomic spin structures assembled by means of scanning tunneling microscopy (STM) provide valuable insight into the understanding of atomic-scale magnetism. Among the major challenges are the detection and subsequent read-out of ultrafast spin dynamics due to a dichotomy in travel speed of these dynamics and the probe tip. Here, we present a device composed of individual Fe atoms that allows for remote detection of spin dynamics. We have characterized the device and used it to detect the presence of spin waves originating from an excitation induced by the STM tip several nanometres away; this may be extended to much longer distances. The device contains a memory element that can be consulted seconds after detection, similar in functionality to e.g. a single photon detector. We performed statistical analysis of the responsiveness to remote spin excitations and corroborated the results using basic calculations of the free evolution of coupled quantum spins.

[1] Department of Quantum Nanoscience, Kavli Institute of Nanoscience, Delft University of Technology, Lorentzweg 1, Delft 2628 CJ, The Netherlands. [2] These authors contributed equally: R.J.G. Elbertse, D. Coffey. ✉email: a.f.otte@tudelft.nl

Spin waves, quantum-mechanically described as magnons, are collective magnetic excitations that, due to their long-distance coherence[1], are considered promising candidates for future spintronic devices[2–5]. In light of the intrinsic quantum nature of these waves, their exact behavior is difficult to predict. Scanning tunneling microscopy (STM)-based atom manipulation allows for the assembly of artificial spin structures[6,7]: a technique that has enabled studies of collective magnetism ranging from the emergence of magnetic bistability[8–10] to spin waves[11], phase transitions[12,13] and topologically protected edge states[14–16]. More recently, the implementation of electron spin resonance (ESR)[17] has led to coherent manipulation of combined atomic spin states[18]. However, by nature of the STM design, in each of these studies the effect of local tip-induced stimuli can only be probed there where they are generated.

For atomic structures that have a static spin state, remote detection schemes exist that make use of a nearby atomic probe[19–21]. In order to remotely probe the dynamic response occurring faster than the tip travel time, one would need to implement a memory unit that stores this response until the tip has had time to arrive. Such memory-based remote detection schemes have been implemented for dynamic processes not based on spin[22,23]. In this work, we present a device that provides memory-based remote detection of spin dynamics in atomic spin structures. By comparing experimental results to calculations we show that the triggering of the detector correlates with the probability of a magnetic excitation induced elsewhere reaching the detector due to free quantum evolution.

Results

Design of spin wave detector. The general design of the spin wave detector, shown in Fig. 1a, is based on Fe atoms on top of Cu_2N. All structures are built in a line along a nitrogen row of the Cu_2N molecular network. This direction coincides with the easy axis of the Fe atom spins, which we treat as effective $S = 2$[24]. During the experiment, we apply a magnetic field $B = 0.5$–1.0 T along this direction in order to maintain spin-polarized tunneling contrast[8]. Structures consist of three parts: an input lead, an output lead and a reset lead. The length of these parts are given as n_{in}, n_{out} and n_{reset}, respectively. For reasons discussed below, the output lead is required to have an even length, whereas the input and reset leads are required to be odd. Throughout this paper, we will use $n_{out} = 8$, $n_{reset} = 3$ and $3 \le n_{in} \le 9$. To describe the structures, we will use the shorthand "n_{in}-n_{out}-n_{reset}"; for example, the structure shown in Fig. 1 will be referred to as "3-8-3".

Neighboring atoms that are part of the same lead are separated by two unit cells of the Cu_2N lattice, which is known to result in an antiferromagnetic coupling with coupling constant $J = 0.7$ meV[25]. Adjacent atoms from different leads are separated by three unit cells. We have determined through inelastic electron tunneling spectroscopy and spin-polarized STM that this separation results in a ferromagnetic coupling -0.05 meV $< J' < 0$ meV. We will use $J' = -0.05$ meV throughout the rest of this paper. See Supplementary Note 1 for a detailed description of the Hamiltonian.

As demonstrated by means of spin-polarized STM in Fig. 1b, the output lead will at any time be in either of two Néel states N_A and N_B. For $n_{out} = 8$, both these states have a lifetime upward of several seconds[8]. We define N_A to be the state where the output atom closest to the input lead is aligned with the field. As n_{in} and n_{reset} are odd, atoms A and A′ (Fig. 1a) will also prefer to align with the field. As a result, when neither the input nor the reset lead is excited, the N_A-state will have a favoured ("happy") coupling to the input lead and an unfavoured ("unhappy") coupling to the reset lead. In this situation, N_A and N_B are degenerate.

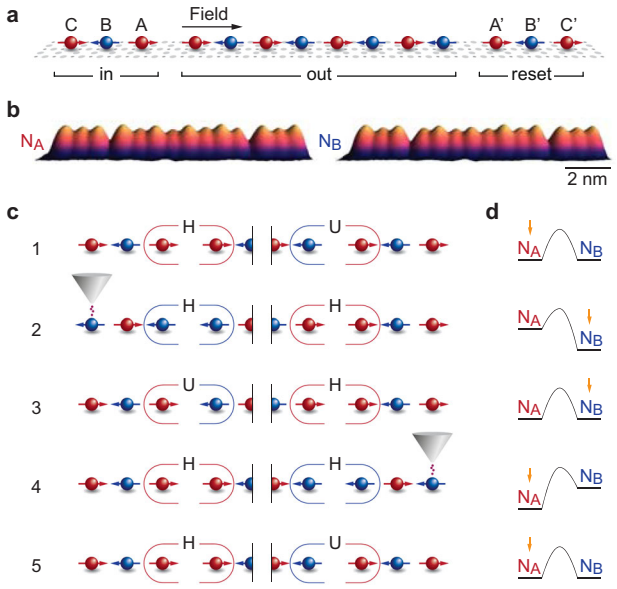

Fig. 1 Operating principle of the spin wave detector. a Schematic overview of a 3-8-3 structure, consisting of an input lead (length $n_{in} = 3$), an output lead ($n_{out} = 8$) and a reset lead ($n_{reset} = 3$). Atoms in the input and reset leads are labeled alphabetically, counting outward from the output lead. **b** Side-view spin-polarized tunneling topographies (1 mV/10 pA at 1.5 K, 0.5 T) of a 3-8-3 in the two allowed states of the output lead: Néel states N_A and N_B. **c** Simplified operation cycle outlined in five steps; see text for more information. Favourable coupling configurations between the output and input/reset are labeled "H" (happy); unfavourable configurations are labeled "U" (unhappy). **d** Simplified energy diagrams showing N_A and N_B in the five situations described in **c**. The arrow indicates the state of the output lead.

An operation cycle consists of the five steps outlined in Fig. 1c. (1) First, the output lead is set to N_A. If this is not the case, the output can be initialized by starting the cycle at step 3. (2) A spin excitation is induced in the input lead, affecting the spin state of atom A. The resulting energy splitting between N_A and N_B causes the system to fall to its ground state N_B. (3) The output lead, consulted by the STM tip, retains its state N_B after the input lead relaxes to its original state. Further actuation on the input lead does not change the output state. (4) A reset is performed by means of a similar excitation on the reset lead, after which (5) the system returns to its initial state N_A. This design provides a ratchet behavior, where the output lead should switch only if the coupling configuration on the input side is "happy", and never if it is "unhappy". In the following experiments, we always start with the tip on the input lead. We then define P_H as the measured probability for the output lead to switch from N_A to N_B, and P_U the probability to switch from N_B to N_A.

In the figure, the input and reset leads are shown to fully invert. However, we emphasize that switching of the output lead would also occur if atom A in step 2 is only partially inverted due to a spin excitation. In fact, as we will discuss below, switches of the output lead can occur already if the magnetization of atom A is changed from $S_z = +2$ to $S_z = +1$, i.e., due to a single short-lived $|\Delta S_z| = 1$ excitation.

Triggering by means of voltage pulses. We have tested the functionality of the device by switching the input lead in two different ways: by means of local spin excitations in the input lead and by means of tip field-induced static inversion of the input lead as a whole. In the first method, we perform voltage pulses on

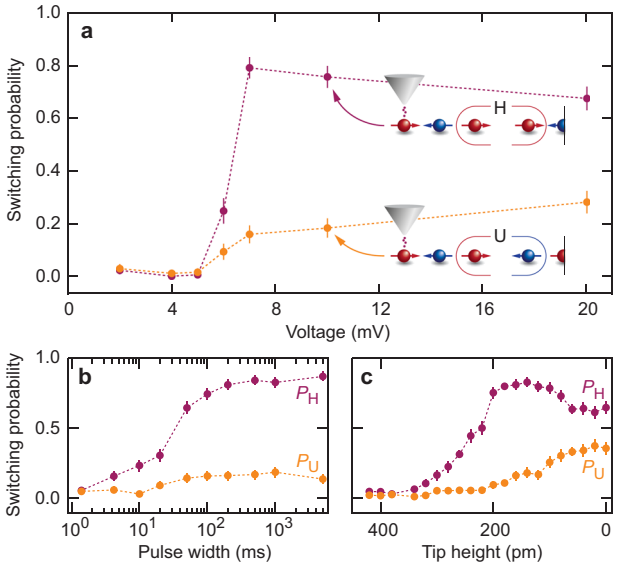

Fig. 2 Switching probabilities as a function of pulse voltage, pulse width and tip height. a Measured values of switching probabilities P_H and P_U as a function of pulse voltage. Data taken with 550 ms pulses at 20 pA (1.5 K, 0.5 T). **b** Measured values of P_H and P_U as a function of pulse width. Data taken at 10 mV, 1.1 pA (1.5 K, 1 T), corresponding to a tip height of 160 pm. Tip heights are defined in comparison to regulating at 1 mV, 3 pA on the Cu_2N island. **c** Measured values of P_H and P_U as a function of tip height. Data taken at 10 mV, pulse width 200 ms (1.5 K, 1 T). All data is based on $N \geq 180$ attempts with the error bars showing 1.5σ for a binomial distribution with μ at the recorded rate. Dashed lines are guides to the eye.

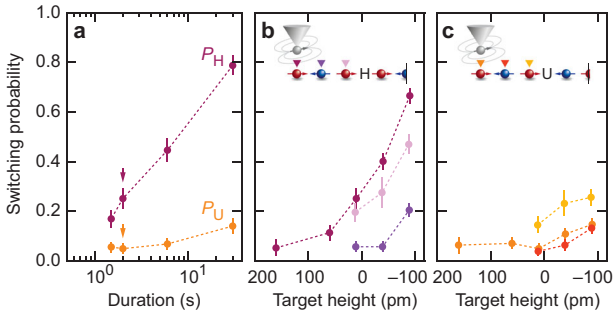

Fig. 3 Switching the input by tip exchange field. a Switching probabilities P_H and P_U as a function of duration at a target tip height of 10 pm, using a bias voltage of 1 mV. Arrows indicate data points that also appear in **b** and **c**. **b** P_H for atoms A, B and C, for a duration of 2 s. Note how atom B is less sensitive to the tip field than atoms A and C. **c** Same as **b** but for P_U. Data in all three subpanels is taken at 1.5 K, 1 T. The error bars show 1.5σ for a binomial distribution with μ at the recorded rate. Dashed lines are guides to the eye.

input atoms, and we characterize the response of the output lead as a function of pulse parameters. Figure 2a shows the switching efficiency after applying voltage pulses of varying height on atom C. Pulse width and tunneling current are kept constant at 550 ms and 20 pA to ensure the same number of electrons for all pulses. We note that this current is too low for the input trimer to spend a significant amount of time in the inverted state. Statistics throughout this paper are based on $N \gtrsim 100$ attempts. During readout of the output lead, the tunnel junction is set to 10 pA at 2 mV, i.e. below the excitation energy.

For small pulse amplitudes, measured switching probabilities are close to zero. However, from ~7 mV, which corresponds to the energy of a spin excitation on atom C from its $S_z = +2$ to its $S_z = +1$ state, increased values are found. Switching probability P_H, for switches originating from the state where the input lead is in the "happy" configuration, reaches 80%. Note that switching probability P_U from the "unhappy" configuration remains much lower, consistent with the expected behavior of the device. For even larger pulse voltages, P_U increases while at the same time P_H decreases. This can be explained in terms of secondary switches during a single pulse back towards the "happy" state. Hence, $P_H + P_U \leq 1$.

Figure 2b, c shows P_H and P_U as a function of pulse width and tip height, respectively. For the settings used in Fig. 2b, we find an approximate switching time $\tau = 25$ ms. As I depends exponentially on tip-sample distance, both graphs show an equivalent range of number of electrons per pulse, $I\Delta t \approx [10^4, 10^8]$. Although both graphs behave similar for small $I\Delta t$, they diverge at higher values: when increasing pulse width, P_H and P_U are found to plateau, while increasing I eventually increases P_U (thus reducing P_H). This suggests a path for switching from the "unhappy" configuration which is based on a multi-excitation process, presumably due to magnon excitations tunneling into the output lead (Supplementary Note 2).

Triggering by means of tip exchange field. In order to exclude the possibility of tunneling magnons, the second method to switch the output lead involves reversing the input lead via controlled exchange coupling with the tip[26]. In this experiment, the voltage is kept below the excitation threshold and the tip is held over an input atom at a certain target height for a certain duration. Figure 3a shows the switching probabilities P_H and P_U as a function of duration for a fixed target height of 10 pm (as compared to regulating at 1 mV, 3 pA on Cu_2N). For this target height we find $\tau \approx 5$ s.

A more detailed investigation is shown in Fig. 3b, c, which shows P_H (P_U) on the different atoms of the input lead as a function of target height. For sufficiently large tip separation, no switching is observed. Bringing the tip closer to the input lead induces switches of the output lead, suggesting that the tip field causes the predominant state of the input lead to switch from $(S_z^C, S_z^B, S_z^A) = (+2, -2, +2)$ to $(-2, +2, -2)$. For target heights down to −100 pm, P_H on atoms A and C increases, whereas P_U does not increase significantly. Likewise, P_H on atom B does not increase significantly beyond P_U. Closer tip extensions are explored in Supplementary Note 3.

We emphasize that the essence of the switching mechanism is different in this second method compared to the first: here the input lead spends a significant amount of time in the fully inverted state, whereas in the first case, $|\Delta S_z| = 1$ excitations on one side of the barrier are the dominant cause for the reduction of the time averaged S_z^A.

Extended input lead and comparison with calculations. Having characterized the sensitivity of the detector to spin excitations on the input lead as described in Fig. 2, we now consider the effect of introducing these excitations at different distances. In Fig. 4a, b, we compare switching measurements for various tip locations on the input lead for $n_{in} = 3$ and 5. Although the measurements on the 5-8-3 indicate a monotonous decrease of the switching probability as a function of distance to the output lead, both for switches from the "happy" and "unhappy" states, measurements on the 3-8-3 show a marked reduction in P_H, and corresponding increase in P_U, when the tip is located on atom B.

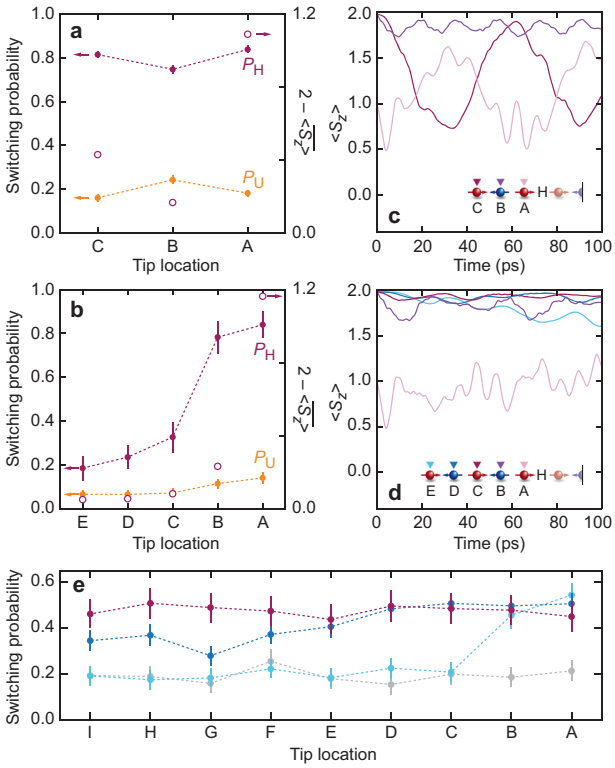

Fig. 4 Switching probabilities as a function of tip location and input length compared to calculations. a Closed circles: switching probabilities P_H and P_U as a function of tip location for $n_{in} = 3$ (10 mV, 2 pA, 550 ms). Open circles: values averaged over the first 20 ps from **c**. Note the different axes used for open and closed circles. **b** Same as **a** but for $n_{in} = 5$ (10 mV, 1.6 pA, 100ms). **c** Time-dependent Schrödinger equation calculations performed on an Fe trimer. The curves show the time evolution of the expectation value of S_z at atom A following a single excitation on each of the input atoms. **d** Same as **c** but for an Fe pentamer. **e** P_H as a function of tip location for $n_{in} = 9$. Different curves correspond to different tip heights: 180 pm (420 fA), 80 pm (4.3 pA) and 30 pm (15.2 pA) for, respectively, light blue, dark blue and magenta. All voltage pulses last 300 ms at 10 mV. The gray curve is taken at 180 pm, 1 mV, for reference. Data in **a**, **b**, **e** are taken at 1.5 K, 1 T. The error bars show 1.5σ for a binomial distribution with μ at the recorded rate. Dashed lines are guides to the eye.

In order to gain insight into this behavior, we performed time-dependent Schrödinger equation calculations simulating the dynamics of the input lead upon an excitation (Fig. 4c, d). In these calculations, we model only the input lead. The coupling to the output lead is modeled by an effective magnetic field on atom A (Supplementary Note 2). First, we initialize the system by finding the ground state of the Hamiltonian. Next, we perform a single spin excitation on one of the input atoms (i.e., we apply the $\hat{S}_+$ or $\hat{S}_-$ operator depending on the position in the antiferromagnetic input lead), after which we apply the time-dependent Schrödinger equation to the resulting state. Plotted are the values $S_z^A(\alpha)$ after an excitation on atom α. Dissipation effects are not considered in these calculations.

Figure 4c, d shows the results of calculations for the first 100 ps on a trimer and pentamer, respectively. As expected, S_z^A values never reach much lower than +1, so a full inversion of the input lead does not occur in these calculations. We estimate the lifetime of an excitation to be ~10 ps (see Supplementary Note 2, not to be confused with the ~1 μs lifetime of the inverted state, see Supplementary Note 4). Therefore, we took the averaged values of $S_z^A(\alpha)$ over the first 20 ps and plotted these as open circled in Fig. 4a, b. As in the experimental data, this results in a deviation from $S_z^A = 2$ that alternates for the trimer, whereas it decreases monotonously for the pentamer. These results suggest that the spin wave detector is able to register unitary spin dynamics.

Finally, in Fig. 4e, we show switching experiments on a 9-8-3 device. Here we find that it is possible to switch the output lead from as far away as 6.8 nm (19 Cu_2N lattice sites). We find that as the current increases, the distance where $P_H \approx 50\%$, the maximum value for this structure, also increases: from 7 lattice sites for $z = 180$ pm to at least 19 lattice sites for $z = 30$ pm. For this structure, the results are compared with a background measurement ($V = 1$ mV, $z = 180$ pm), which yields a minimum switching rate of ~20%. We attribute this increased base switching probability to longer lifetime of the input lead (in the order of 1 s), therefore spending extended periods of time in the inverted state, even in the absence of excitations.

Discussion

In summary, we have developed an atomic device that can be used to detect dynamic and nonlocal spin phenomena such as magnons. We have tested the device for its sensitivity to spin excitations, as well as a complete inversion of the input lead. We have shown that the device is sensitive to spin excitations originating up to 9 atoms away. In subsequent experiments, the input lead may be replaced by more exotic spin architectures. This method thereby provides a tool in studying dynamic spin processes on the atomic scale.

Methods

We used a UNISOKU USM-1300s ^{3}He STM system, operating at 1.5 K and $B = 0.5$–1 T in the plane of the sample, along the axis of the structures. The Cu_2N/Cu_3Au(100) sample was prepared as described by Gobeil et al.[27]. The tip is prepared as in Loth et al.[8]. Fe atoms were picked up from the Cu_2N by using bias pulses of ~1 V at (regulation 100 pA, 20 mV, then move −300 pm) and dropped at −600 μV with the tip gradually nearing the surface until a change in current is observed. The Fe was subsequently maneuvered into place with a pulse of ~1 V at (100 pA, 20 mV). Calculations were performed using QuTip[28,29], a library for Python. See Supplementary Note 6 for a more detailed description of the data acquisition technique, and Supplementary Note 5 for possibilities on even faster data acquisition.

Data availability

All data presented in this paper is publicly available via digital object identifier (DOI) 10.5281/zenodo.3759448. Included in the open data folder are the raw data and the Python scripts to process the data, to reproduce Figs. 2, 3 and 4. Figure 1 does not include experimental data.

Received: 23 January 2020; Accepted: 30 April 2020;
Published online: 25 May 2020

References

1. Lenk, B., Ulrichs, H., Garbs, F. & Münzenberg, M. The building blocks of magnonics. *Phys. Rep.* **507**, 107–136 (2011).
2. Chumak, A. V., Vasyuchka, V. I., Serga, A. A. & Hillebrands, B. Magnon spintronics. *Nat. Phys.* **11**, 453–461 (2015).
3. Khajetoorians, A. A., Wiebe, J., Chilian, B. & Wiesendanger, R. Realizing all-spin-based logic operations atom by atom. *Science* **332**, 1062–1064 (2011).
4. Han, J., Zhang, P., Hou, J. T., Siddiqui, S. A. & Liu, L. Mutual control of coherent spin waves and magnetic domain walls in a magnonic device. *Science* **366**, 1121–1125 (2019).
5. Wang, Y. et al. Magnetization switching by magnon-mediated spin torque through an antiferromagnetic insulator. *Science* **366**, 1125–1128 (2019).
6. Hirjibehedin, C. F., Lutz, C. P. & Heinrich, A. J. Spin coupling in engineered atomic structures. *Science* **312**, 1021–1024 (2006).
7. Choi, D.-J. et al. Colloquium: Atomic spin chains on surfaces. *Rev. Mod. Phys.* **91**, 041001 (2019).
8. Loth, S., Baumann, S., Lutz, C. P., Eigler, D. M. & Heinrich, A. J. Bistability in atomic-scale antiferromagnets. *Science* **335**, 196–199 (2012).

9. Loth, S., Etzkorn, M., Lutz, C. P., Eigler, D. M. & Heinrich, A. J. Measurement of fast electron spin relaxation times with atomic resolution. *Science* **329**, 1628–1630 (2010).
10. Khajetoorians, A. A. et al. Current-driven spin dynamics of artificially constructed quantum magnets. *Science* **339**, 55–59 (2013).
11. Spinelli, A., Bryant, B., Delgado, F., Fernández-Rossier, J. & Otte, A. F. Imaging of spin waves in atomically designed nanomagnets. *Nat. Mater.* **13**, 782–785 (2014).
12. Khajetoorians, A. A. et al. Atom-by-atom engineering and magnetometry of tailored nanomagnets. *Nat. Phys.* **8**, 497–503 (2012).
13. Toskovic, R. et al. Atomic spin-chain realization of a model for quantum criticality. *Nat. Phys.* **12**, 656–660 (2016).
14. Nadj-Perge, S. et al. Observation of majorana fermions in ferromagnetic atomic chains on a superconductor. *Science* **346**, 602–607 (2014).
15. Kim, H. et al. Toward tailoring majorana bound states in artificially constructed magnetic atom chains on elemental superconductors. *Sci. Adv.* **4**, eaar5251 (2018).
16. Ruby, M. et al. End states and subgap structure in proximity-coupled chains of magnetic adatoms. *Phys. Rev. Lett.* **115**, 197204 (2015).
17. Baumann, S. et al. Electron paramagnetic resonance of individual atoms on a surface. *Science* **350**, 417–420 (2015).
18. Yang, K. et al. Coherent spin manipulation of individual atoms on a surface. *Science* **366**, 509–512 (2019).
19. Yan, S. et al. Nonlocally sensing the magnetic states of nanoscale antiferromagnets with an atomic spin sensor. *Sci. Adv.* **3**, e1603137 (2017).
20. Natterer, F. D. et al. Reading and writing single-atom magnets. *Nature* **543**, 226–228 (2017).
21. Hermenau, J. et al. Stabilizing spin systems via symmetrically tailored RKKY interactions. *Nat. Commun.* **10**, 2565 (2019).
22. Kügel, J. et al. Remote single-molecule switching: Identification and nanoengineering of hot electron-induced tautomerization. *Nano Lett.* **17**, 5106–5112 (2017).
23. Heinrich, A. J., Lutz, C. P., Gupta, J. A. & Eigler, D. M. Molecule cascades. *Science* **298**, 1381–1387 (2002).
24. Hirjibehedin, C. F. et al. Large magnetic anisotropy of a single atomic spin embedded in a surface molecular network. *Science* **317**, 1199–1203 (2007).
25. Bryant, B., Spinelli, A., Wagenaar, J. J. T., Gerrits, M. & Otte, A. F. Local control of single atom magnetocrystalline anisotropy. *Phys. Rev. Lett.* **111**, 127203 (2013).
26. Yan, S., Choi, D.-J., Burgess, J. A. J., Rolf-Pissarczyk, S. & Loth, S. Control of quantum magnets by atomic exchange bias. *Nat. Nanotechnol.* **10**, 40–45 (2014).
27. Gobeil, J., Coffey, D., Wang, S.-J. & Otte, A. F. Large insulating nitride islands on Cu_3Au as a template for atomic spin structures. *Surf. Sci.* **679**, 202–206 (2019).
28. Johansson, J., Nation, P. & Nori, F. QuTiP: an open-source Python framework for the dynamics of open quantum systems. *Comput. Phys. Commun.* **183**, 1760–1772 (2012).
29. Johansson, J., Nation, P. & Nori, F. QuTiP 2: a Python framework for the dynamics of open quantum systems. *Comput. Phys. Commun.* **184**, 1234–1240 (2013).

Acknowledgements

We acknowledge support from the Netherlands Organisation for Scientific Research (NWO) and from the European Research Council (ERC Starting Grant 676895 "SPIN-CAD"), and thank J. Fernández-Rossier for discussion.

Author contributions

D.C. and A.F.O. designed the experiment. R.J.G.E., D.C. and J.G. performed the experiments. R.J.G.E. analyzed the data, making use of code written by J.G. The manuscript was written by R.J.G.E., D.C. and A.F.O.

Competing Interests

The authors declare no competing interests.

Additional information

Supplementary information is available for this paper at https://doi.org/10.1038/s42005-020-0361-z.

Correspondence and requests for materials should be addressed to A.F.O.

Reprints and permission information is available at http://www.nature.com/reprints

Publisher's note Springer Nature remains neutral with regard to jurisdictional claims in published maps and institutional affiliations.